[CI] 492 GHz Study of the Galactic Center

B. Mookerjea[1], C. L. Martin[2], J. Stutzki[1], A. A. Stark[2], A. P. Lane[2], W. M. Walsh[2] and , K. Xiao[2]

[1] KOSMA, I. Physikalisches Institut, Universität zu Köln, Zülpicher Strasse 77, D 50937, Köln,Germany bhaswati,stutzki@ph1.uni-koeln.de

[2] Harvard Smithsonian Center for Astrophysics, Cambridge, USA cmartin,aas,alane,wwalsh,kxiao@cfa.harvard.edu

1 Introduction

Molecular clouds consist mostly of clumps, the surfaces of which are illuminated by UV radiation resulting in Photon Dominated Regions (PDR's), which constitute a large fraction of the molecular material (and the neutral ISM). In the PDRs the dominant carbon bearing species changes from C^+ to C^0 to CO. Neutral carbon has two fine structure transitions at 492 GHz ($^3P_1 \rightarrow ^3P_0$) and 809 GHz ($^3P_2 \rightarrow ^3P_1$). The upper state of the transition at 492 GHz is only 23 K above ground and has a critical density of 1000 cm^{-3} for collisions with H_2 molecules. This implies that [CI] is easily excited and also the line is easily detectable even when emitted by moderate density interstellar gas exposed only to a radiation field equal to the mean interstellar radiation field in the solar neighborhood. We present results of preliminary analysis of a large scale 492 GHz [CI] survey of the Galactic center. We present first detection of a spatially extended narrow absorption feature, only weakly seen in ^{12}CO and ^{13}CO, that is due to cold foreground material along lines of sight in the direction of Sgr C.

2 The [CI] Data

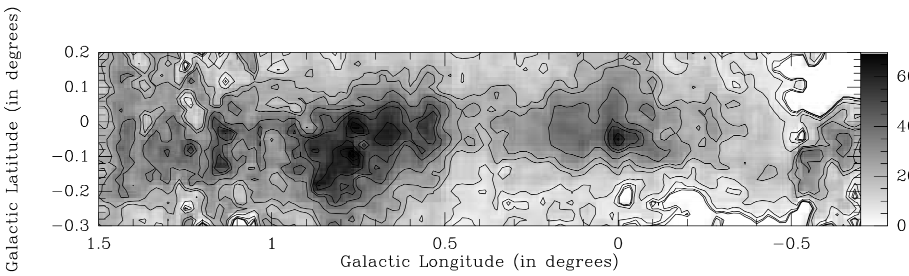

Fig. 1. Integrated intensity map of [CI] at 492 GHz emission from the Galactic center

Figure 1 shows the map of the integrated [CI] intensity as observed with the AST/RO telescope by Martin et al. 2003 (and A. A. Stark et al. in this volume). The [CI] data has been analyzed in combination with the Bell Labs (7m) ^{12}CO(1-0), ^{12}CO (1-0) and CS(2-1) data (Stark et al. 1989 & Bally et al. 1987) and ^{12}CO (4-3) data taken with AST/RO (Martin et al. 2003). For direct comparison, all datasets have been smoothed to the same angular resolution of $2'$ and gridded on a $1'$ grid.

3 Line Intensity Ratios for selected emission features

We have selected 6 emission features corresponding to the peak intensities in the regions chosen based on the position-velocity diagram. Figure 2 shows the spectra corresponding to these emission features and Table 1 list positions and line intensity ratios calculated at each position.

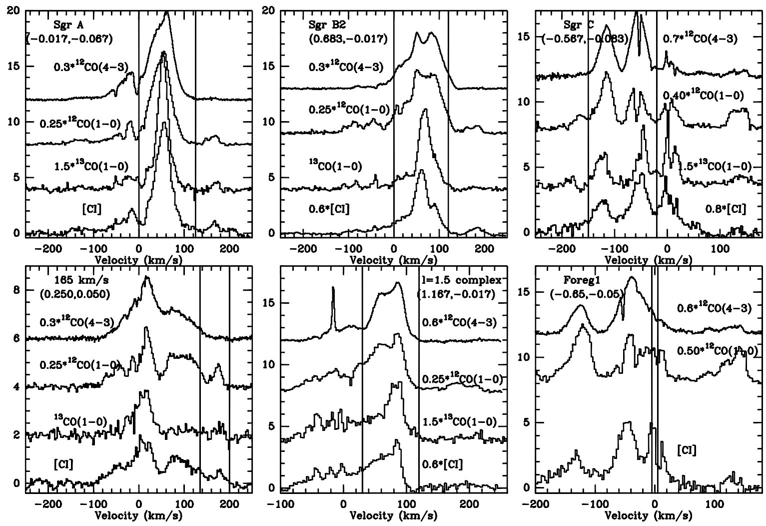

Fig. 2. Observed spectra for selected emission features in the Galactic center. Spectra have been drawn with offsets for better visibility. The vertical lines correspond to the velocity ranges over which the integrated intensities are calculated.

The [CI]/CO(1-0) is fairly constant for most regions, except for Sgr C and the foreground emission feature. The CO(1-0)/CO(4-3) ratio is, within limits of the error, identical for Sgr A, B2 and C and the value, $\sim 1.3\pm0.2$) , reflects optical thickness of the emission. At the other three positions the values deviate substantially. This is in contrast to the observed CO(1-0)/CO(2-1) ratio of ~ 1 for the entire Galactic center (Sawada et al. 2001). Optically thin ^{12}CO

Table 1. Line intensity ratios for selected emission features in the Galactic Center.

Feature	(l, b)	$\frac{[CI]}{CO(1-0)}$	$\frac{[CI]}{^{13}CO(1-0)}$	$\frac{[CI]}{CO(4-3)}$	$\frac{CO(1-0)}{CO(4-3)}$	$\frac{^{13}CO(1-0)}{CO(4-3)}$	$\frac{^{13}CO(1-0)}{CO(1-0)}$
Sgr A	-0.017,-0.067	0.26	1.80	0.30	1.14	0.17	0.15
Sgr B2	0.683,-0.017	0.27	1.62	0.37	1.35	0.23	0.17
Sgr C	-0.567,-0.083	0.61	4.61	0.88	1.44	0.19	0.13
165 km s^{-1}	0.250,0.050	0.24	4.15	1.32	5.53	0.32	0.06
l= 1.5	1.167,-0.017	0.28	2.07	0.70	2.51	0.34	0.13
Fground1	-0.650,-0.050	0.82	...	1.86	2.26	...	...

emission is evident in the 165 km/s arm, l=1.5 complex and the Foreground emission feature, where the CO(1-0)/CO(4-3) differs substantially from unity, and the $^{13}CO/^{12}CO(1\text{-}0)$ ratio are low (between 0.06 and 0.13).

Preliminary estimates using calculations based on Escape Probability method (Stutzki & Winnewisser 1985) as well as detailed models for PDRs (Störzer et al. 1996) suggest that the density at Sgr A (and Sgr B2) is $\sim 10^{4.5}$cm^{-3}, while the density at Sgr C is $\sim 10^{3.5}$cm^{-3}.

4 Detection of extended foreground absorption

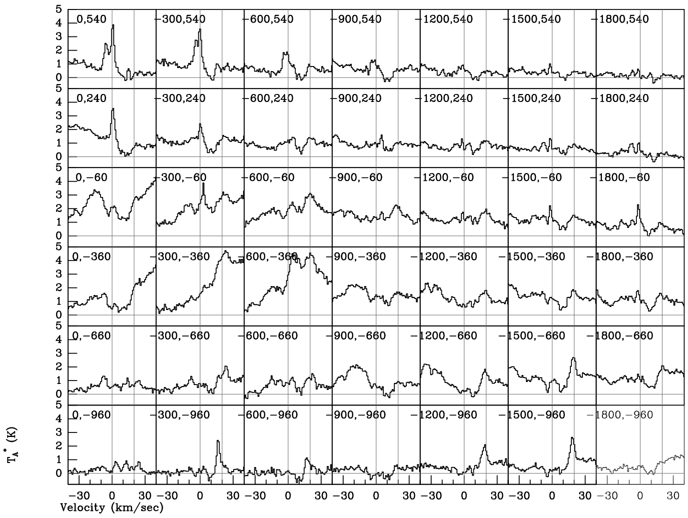

Fig. 3. [CI] spectra showing the extent of the absorption dip. Each position corresponds to a $5' \times 5'$ average centered at the position (offsets in arcseconds) indicated in the panels. Vertical lines are drawn to provide guidance to identify the absorption feature

The [CI] observations (Figure 3) presented here confirm the large spatial extent (at least $35' \times 35'$) of a spectrally narrow absorption feature extending from $v_{\rm lsr}$ =5 to 15 km s^{-1} toward the broad line emission from Sgr C. This feature was first detected at a few positions by Staguhn et al. (1997). The absorption feature clearly shows two velocity components centered at 8 km/s and 12.5 km/s with velocity widths of 4.5 and 3.5 km/s respectively. The relative strengths of the two components vary with position. For quantitative analysis of the absorption feature we spatially average $5' \times 5'$ regions to improve the S/N ratio.

We use a method similar to that outlined by Staguhn et al. (1997) to derive the excitation temperature and column density of the absorbing foreground cloud. Using the geometry explained in Figure 5 of Staguhn et al. (1997) and the constraint that the line is seen in absorption and the beam filling factor of the foreground cloud (α_f) has to be between 0 and 1 we arrive at the following expression for the excitation temperature ($T_{ex,f}$) for the foreground cloud:

$$J_\nu(T_{ex,f}) \leq T_{mb,bg} + J_\nu(2.7\ K) + T_{absorb} \tag{1}$$

where $J_\nu(T) \equiv (h\nu/k)(e^{h\nu/kT} - 1)^{-1}$ is the Rayleigh Jean's function, T_{absorb} is the (negative) antenna temperature corresponding to the absorption feature and $T_{mb,bg}$ is the observed brightness temperature of the background emission.

The upper limits of $T_{ex,f}$ calculated as above for the two absorption components in [CI] range between 3 to 10 K. Using these $T_{ex,f}$ the lower limits for the [C I] column densities calculated at all positions for both components are equal to a few times 10^{17} cm^{-2}.

The ^{12}CO(1-0) data for the same region shows only one absorption component centered around 12.1 km/s and with a width of 3.5 km/s. Using an analysis similar to that for the [CI] data we arrive at excitation temperatures between 4 to 15 K and CO column densities between 10^{15} to 10^{16} cm^{-2}. Both components of the absorption feature have marginally detected at a few positions in the ^{13}CO(1-0) data and preliminary analysis provides an excitation temperature of 3.5 K and a ^{13}CO column density of $\sim 10^{15}$ cm^{-2}.

The reason for the apparent discrepancy between the column densities of CI and CO and the usual relative abundance of these species is not understood. While the ^{12}CO is likely to be optically thick, this is less true of ^{13}CO. Possible explanations for the underabundance of CO and its isotopomers include dissociation or freezing out of CO in the foreground cloud.

This work was supported by the DFG within grant SFB-494 and in part by U.S. NSF grant OPP0126090.